Development of Microporous Structure and its Application to Optical Film for Cellulose Triacetate Containing Diisodecyl Adipate

Hikaru Shimada, Shogo Nobukawa, and Masayuki Yamaguchi*

School of Materials Science, Japan Advanced Institute of Science and Technology
1-1 Asahidai, Nomi, Ishikawa 923-1292, Japan

*To whom correspondence should be addressed:
1-1 Asahidai, Nomi, Ishikawa 923-1292 JAPAN
E-mail: m_yama@jaist.ac.jp
Phone +81-761-51-1621
Fax +81-761-51-1625

Abstract

Phase separation in plasticized cellulose triacetate (CTA) films is investigated to produce a microporous film that can be used in optical devices. Hot-stretched CTA films containing diisodecyl adipate (DIDA) show negative orientation birefringence similar to the hot-stretched pure CTA. After extracting DIDA from the stretched films by immersion into an organic solvent, however, the films exhibit positive birefringence. Moreover, the magnitude of the birefringence increases with the wavelength, known as extraordinary dispersion, which is an essential property in the preparation of an ideal quarter-wave plate. Numerous ellipsoidal pores with micro-scale were detected in the film after the immersion, indicating that DIDA were segregated and formed ellipsoidal domains in the CTA matrix during annealing and stretching. These results indicate that extraordinary wavelength dispersion is given by the combinations of orientation birefringence from CTA and form birefringence from micropores. Furthermore, it was found that annealing time and stretching condition affect the phase separation as well as the shape and size of pores.

Keywords: Cellulose triacetate; Optical Film; Birefringence; Microporous structure; Blends

1. Introduction

Microporous materials have been studied intensively these days because of their application in the industry and their future potential of additional functions for various products (Silverstein et al., 2011). In general, micropores are responsible for some advantages such as increase in the surface area and penetration distance from one surface to another, besides weight saving. Therefore, microporous materials are used as absorbent, catalyst, and so on (Wakao & Smith, 1964; Arenas & Crocker, 2010). Moreover, microporous materials are expected to expand the applications recently, because advanced functions attributed to micropores have been discovered. As an example of their application in thermal insulation, it is desired that the pore size should be smaller than the mean free path of air, i.e., ca. 60 nm (Clyne et al., 2006). Moreover, micropores having appropriate size are also required for biomaterials such as vehicle for drug and gene delivery (Selvam et al., 2009). In the case of the Lithium ion battery, a separator has to have microporous structure, which should provide the self-shuttering function at high temperature (Love, 2011; Phulkerd et al., 2013). These applications indicate that well-controlled micropores have a great potential to produce functional materials, and it is necessary to control the size and amount of micropores in order to be used in such applications.

There are several methods to produce porous materials: fiber bonding, solvent casting/particulate leaching, gas foaming, plastic deformation, and phase separation/emulsification (Mikos & Temenoff, 2000; Selvam et al. 2009; Phulkerd et al., 2013; Samthong et al., 2014). In the phase separation method, a component of dispersed phase is removed after separation to produce

62 pores. Therefore, the miscibility is important to control the structure.

63 As well known, free energy of mixing ΔG_{mix} is expressed as,

64 $$\Delta G_{mix} = \Delta H_{mix} - T\Delta S_{mix} \quad (1)$$

65 where ΔH_{mix} is the mixing enthalpy and ΔS_{mix} is the mixing entropy. Equation (1) demonstrates that
66 the temperature and the interaction parameter which decides ΔH_{mix} are the basic parameters to be
67 considered. These factors are important for the formation of pores. For example, phase separation
68 should occur by spinodal decomposition in order to obtain large number of fine pores (Olmsted et al.,
69 1998; Matsuba et al. 1999). In addition, phase separation can occur by several factors other than
70 temperature change and interaction of materials (Rangel-Nafaile et al., 1984; Lee et al., 2004).
71 Specifically, the orientation of polymer chains by stretching causes the phase separation originating
72 from entropy loss of miscible system, i.e., the so-called flow-induced phase separation (Yanase et al.,
73 1991). On the contrary, some polymer blends show flow-induced mixing by the reduction of
74 concentration fluctuation (Mazich & Carr, 1983; Hindawi et al., 1990). In order to control the pore
75 growth, the effect of these factors must be revealed.

76 Here, we focus on the mechanism of phase separation to produce the porous material. Cellulose
77 triacetate (CTA), one of the general-purpose polymers for optical films, is used as a matrix polymer.
78 Because CTA exhibits excellent transparency and heat resistance (Songsurang et al., 2012), the films
79 are used for optical applications in industry. In this paper, the micropores in an oriented CTA film are
80 provided using a plasticizer which has poor miscibility with CTA, and this film can be employed as a

multi-band wave plate, one of the functional optical films required for an advanced display. In this study, the microporous structure using heat-induced and flow-induced phase separation is investigated.

2. Experimental

2.1. Materials

Cellulose triacetate (CTA) (Daicel, LT-35) was employed as the matrix polymer. The degree of acetylation per a pyranose unit is 2.9. The weight-average M_w and the number-average molecular weights M_n were 1.3 x 10^5 and 3.5 x 10^5, determined by a gel permeation chromatography (Tosoh, HLC-8020) with TSK-GEL® GMHXL as a polystyrene standard. Commercially available plasticizers such as diethyl phthalate (DEP) and diisodecyl adipate (DIDA), which are involatile liquid, were used in this study without further purification. Both of them were produced by Daihachi Chemical Industry. The structure and properties of CTA and plasticizers are shown in Figure 1 and Table 1. The values of refractive indices at 633 nm of the plasticizers are close to that of CTA at room temperature.

The solubility parameters calculated by the group contribution method (Grulke, 2003) indicate that DIDA has poor miscibility with CTA as compared with DEP.

[Figure 1] [Table 1]

100 *2.2. Film Preparation*

101 The films were prepared by a solution-cast method. CTA and plasticizers with 10/1 weight ratio
102 were dissolved into mixture solvent of dichloromethane and methanol with 9/1 weight ratio. It was
103 confirmed that the solvent dissolves CTA rapidly. The solution containing 4 wt% of CTA was
104 evaporated at room temperature to obtain the films with 70 μm thickness.

105 The films were uni-axially stretched at various strain rates of 0.01, 0.05, and 0.10 s^{-1} by a tensile
106 machine (UBM, DVE-3) with a temperature controller. The hot-stretching was performed after
107 holding at the drawing temperature (T_{draw}) for 10 min. T_{draw}, shown in Table 2, was decided to obtain
108 the same stress level for all samples. The hot-stretched films were immediately quenched by cold air
109 blowing at a draw ratio of 1.5 to avoid relaxation of molecular orientation. Furthermore, the
110 annealing treatment of non-stretched films was performed at 208 ^{o}C, i.e., T_{draw} for CTA/DIDA, for 1,
111 10, and 20 min to clarify the effect of thermal history on the morphology development.

112 The films were immersed into methanol for 6 hours to remove plasticizers. Then, they were
113 dried in vacuo at room temperature. The removal of plasticizers was confirmed from spectra of
114 infrared absorption spectrometry (Perkin Elmer, Spectrum 100).

115

116 *2.3. Measurements*

117 Dynamic mechanical analysis (DMA) for the solution-cast films of CTA and plasticized CTA
118 was performed to measure oscillatory tensile modulus at 10 Hz as a function of temperature using a

119 dynamic mechanical analyzer (UBM, DVE-E4000) from -100 to 250 ^{o}C with a heating rate of
120 2 ^{o}C min^{-1}. The glass transition temperature T_g was estimated from a peak temperature of tensile loss
121 modulus E'' and shown in Table 2.

122 [Table 2]

123 The birefringence Δn of films was measured by an optical birefringence analyzer (Oji Scientific
124 Instruments, KOBRA-WPR) as a function of wavelength by changing color filters. Prior to the
125 measurement of birefringence, the films were kept in a humidic chamber (Yamato, IG420) at 25 ^{o}C
126 and 50 %RH for one night to avoid the moisture effect on the optical properties (Abd Manaf et al.,
127 2011a). Birefringence is calculated by the following equation,

128 $$\Delta n = n_x - n_y \quad (2)$$

129 where x is the stretching direction and y is the vertical direction from x in plane.

130 The light transmittance of films was measured by an ultraviolet-visible absorption spectroscopy
131 (Perkin Elmer, Lambda 25) with the wavelength from 200 nm to 700 nm at room temperature. The
132 total transmittance in the visible wavelength, i.e., 400-700 nm, was calculated to evaluate the
133 transparency of the films.

134 The morphology of the films was observed by a scanning electron microscope (SEM) (Hitachi,
135 S4100) with an acceleration voltage of 20 kV. Prior to the SEM observation, the surface of films was
136 coated with Pt-Pd by an ion-sputter machine (Hitachi, E1010).

137

3. Results and Discussion

3.1. Miscibility of plasticizers with CTA

The miscibility of CTA and the plasticizers was examined by the dynamic mechanical properties. Figure 2 shows the temperature dependence of tensile storage moduli *E* ' and *E*" for the solution-cast films of pure CTA and CTA with 10 phr of the plasticizer. The dynamic mechanical properties of CTA/DEP demonstrate that T_g of CTA is shifted to lower temperature by DEP addition, suggesting the plasticizing effect of DEP. On the other hand, DIDA hardly affects T_g. Considering that the solidification temperature of DIDA is lower than that of DEP, the result indicates that DIDA is immiscible with CTA. Furthermore, it should be mentioned that the CTA/DIDA film becomes opaque after the measurement of the dynamic mechanical properties owing to the light scattering originated from the phase separated morphology, although the virgin sample without thermal history, i.e., the solution-cast film, is transparent. These results indicate that the CTA/DIDA blend has lower critical solution temperature. During the measurement, DIDA is segregated and thus forms domains at high temperature. In other words, DIDA is dissolved into CTA in the molecular scale prior to the thermal history of the dynamic mechanical measurement. As a result, the magnitude of *E'* in the glassy region for the CTA/DIDA film is almost identical to that for the CTA/DEP film. Although there is a slight possibility that a small amount of DIDA is segregated at the final stage of evaporation for CTA/DIDA, the domains, if there, could be significantly small.

[Figure 2]

157

158 *3.2. Orientation birefringence of CTA and plasticized CTA*

159 The films were stretched above T_g. As well known, the stretched films of polymeric materials
160 show the orientation birefringence originated from polarizability anisotropy by molecular orientation.
161 In order to compare the orientation birefringence of stretched films, the stress at the hot-stretching
162 was adjusted to be the same by adjusting the drawing temperature. This is reasonable because the
163 orientation birefringence Δn_o of a polymer is proportional to the stress σ as follows (Treloar, 1958),

164 $$\Delta n_o = C\sigma \qquad (3)$$

165 where C is the stress-optical coefficient.

166 The stress-strain curves of CTA and plasticized CTA at a strain rate of 0.05 s^{-1} are shown in
167 Figure 3. All films show the same stress level, indicating that the orientation of CTA chains in the
168 blend is identical to that in the pure CTA.

169 [Figure 3]

170 The birefringence of the stretched films is shown in Figure 4. The hot-stretched CTA/plasticizer
171 films show negative birefringence with ordinary wavelength dispersion, as similar to that of the pure
172 CTA film; the absolute value of the birefringence decreases with wavelength. Furthermore, the
173 addition of DEP greatly affects the birefringence. This is attributed to the Nematic interaction that
174 occurs in a miscible system (Abd Manaf et al., 2011b). In the case of DIDA, this phenomenon is not
175 so obvious as compared with DEP. This is reasonable because DIDA is not fully miscible with CTA

176 at the drawing temperature. Instead of the cooperative molecular orientation, the segregated DIDA
177 droplets are deformed to the stretching direction. As a result, form birefringence, originated from
178 anisotropy of refractive indices in anisotropic structure, is expected (Born & Wolf, 1964). However,
179 the refractive indices of CTA and plasticizers are almost the same as shown in Table 1. Therefore, the
180 form birefringence originated from ellipsoidal DIDA droplets hardly affects the total birefringence of
181 a stretched film. Moreover, this result indicates that both plasticizers cannot change the wavelength
182 dispersion of CTA from ordinary wavelength dispersion.

183 [Figure 4]

184

185 *3.3. Removal of plasticizers*

186 The plasticizers were extracted from the stretched films by immersion into methanol. Although
187 the transparency barely changes by the methanol immersion followed by the drying process, which is
188 shown later, numerous prolonged pores to the stretching direction are detected by SEM in the
189 CTA/DIDA film as shown in Figure 5(a). It is confirmed by the weight measurements and FT-IR
190 spectra that DIDA is fully extracted by the solvent. Therefore, the film in Figure 5(a) is composed of
191 pure CTA with the voids. Considering that voids are hardly detected in the CTA/DEP film after
192 methanol immersion as shown in Figure 5(b), the voids in Figure 5(a) are the dispersed phase of
193 DIDA before immersion.

194 [Figure 5]

195 It is known that the homogeneous distribution of ellipsoidal dispersions with different refractive
196 index provides the form birefringence. Although the form birefringence prior to the methanol
197 immersion can be neglected due to the small difference in the refractive indices, it becomes a large
198 value after the extraction process. Figure 6 shows the birefringence of the stretched film before/after
199 the extraction. Birefringence of a pure CTA film is not affected by the immersion, suggesting that the
200 orientation of CTA chains is not relaxed by the process. In the case of the miscible system, the
201 birefringence approaches that of pure CTA as discussed in the previous paper (Abd Manaf et al.,
202 2011b).

203 On the contrary, in the case of the immiscible CTA/ DIDA blend, the birefringence of the film
204 dramatically changes from negative to positive with extraordinary wavelength dispersion;
205 birefringence increases with the wavelength. This result indicates the great contribution of form
206 birefringence originated from anisotropic pores as illustrated in Figure 7. Since the extraordinary
207 wavelength dispersion is required in industry for advanced optical devices such as organic
208 electroluminescence (EL) display, optical pick-up units, and three dimensional (3D) display
209 (Yamaguchi et al., 2009), the results in Figure 6 should be noted.

210 Assuming that the refractive index of the void, i.e., air, is unity, the form birefringence Δn_F
211 ascribed to voids is given by the following equation (Richter et al., 1995),

212 $$\Delta n_F = A - \frac{n}{A} \tag{4}$$

213 $$A = \left[(1 - f)n^2 + f\right]^{1/2} \tag{5}$$

where n is the refractive index of CTA and f is the filling factor of voids, i.e., the ratio of the void length to the distance between neighbor voids in the stretching direction.

Since the stretching condition affects the shape of voids, i.e., the filling factor, it has to be considered seriously to control the birefringence.

[Figure 6] [Figure 7]

3.4. Mechanism of phase separation

The growth of DIDA droplets at the heating and/or stretching processes is investigated by SEM observation using the films after the DIDA extraction. As shown in Figure 8(a), pores are not found in the cast-film, which corresponds with the high level of transparency. After annealing at the drawing temperature, small pores are detected in the film with a low volume fraction, indicating that the phase separation occurs at high temperature to some degree. Moreover, the pores become larger after stretching with the deformation to the stretching direction. The enlargement of each void and the total volume fraction of voids indicates the flow-induced phase separation (Yanase et al., 1991). Therefore, the thermal history and the stretching rate should be considered at the hot-stretching to control the porous structure, and thus, the birefringence.

[Figure 8]

The effect of heating and stretching on phase separation is investigated by light transmittance using the films before/after extracted DIDA. Table 3 shows the total transmittance in the range of

400-700 nm of UV-Vis spectra of the annealed films. As shown here, the transmittance of CTA/DIDA decreases with the annealing time, as compared with that of pure CTA. It suggests that DIDA is segregated from CTA and forms domains during heating.

[Table 3]

Figure 9 shows the stress-strain curves of pure CTA and CTA/DIDA films with various strain rates: 0.01, 0.05, and 0.10 s^{-1} after 10 min annealing. As increasing the strain rate, the stress level increases, suggesting that the chain orientation of CTA is enhanced. The total transmittance of the stretched films after extraction is around 87-88%, irrespective of the strain rates. The value is slightly lower than that for the unstretched film, which corresponds with SEM observation.

[Figure 9]

Figure 10 shows the birefringence of the stretched film after extraction. Although the stress level is different, the pure CTA shows almost the same orientation birefringence. Because polarizability anisotropy of the main chain of CTA is small as compared with the acetyl group in side chain (Yamaguchi et al., 2009), the orientation birefringence is hardly affected by the orientation of main chains. In contrast, birefringence of the extracted CTA/DIDA films increases with the strain rate, although it hardly affects the transparency. The enhanced form birefringence will be attributed to the prolonged voids, which is determined by the chain orientation of CTA.

[Figure 10]

4. Conclusion

We focus on microporous structure formation in CTA films utilizing phase separation of a plasticizer in the polymer. The hot-stretched CTA film containing plasticizers shows negative birefringence with ordinary wavelength dispersion, as similar to that of the pure CTA film. However, the birefringence of the films with an immiscible plasticizer, DIDA, changes from negative to positive after the removal of the plasticizer. In addition, the film exhibits extraordinary wavelength dispersion. The SEM observation reveals that the film contains numerous ellipsoidal pores with nanoscale, which provide the form birefringence as a positive value. This is a new material design of the film showing extraordinary wavelength dispersion, i.e., high performance retardation film. Further, the important phenomena to produce the microporous structure are demonstrated such as phase diagram (LCST) and flow-induced phase separation.

References

Abd Manaf, M. E.,Tsuji, M., Nobukawa, S. & Yamaguchi, M. (2011a). Effect of moisture on the orientation birefringence of cellulose esters. Polymers, 3(2), 955-966.

Abd Manaf, M. E., Tsuji, M., Shiroyama, Y., & Yamaguchi, M. (2011b). Wavelength dispersion of orientation birefringence for cellulose esters containing tricresyl phosphate, Macromolecules, 44(10), 3942–3949.

Arenas, J. P. & Crocker, M. J. (2010). Recent trends in porous sound-absorbing materials, Sound Vib. 12-17.

Born, M. & Wolf, E. (1964). Principles of Optics, 2nd ed., Chap.14, Oxform, Pergamon.

Clyne, T. W., Golosnoy, I. O., Tan, J. C. & Markaki, A. E. (2006). Porous materials for thermal

management under extreme conditions, Phil. Trans. Roy. Soc. A 364(1838), 125–146.

Grulke, E. A. Solubility parameter values, Chapter 7, Polymer Handbook, Vol. 2, 2003, Wiley-Interscience, New York, 675-711.

Hindawi, I.; Higgins, J. S.; Galambos, A. F. & Weiss, R. A. (1990). Flow-induced mixing of blends of poly(ethylene-vinyl acetate) and solution chlorinated polyethylene. Macromolecules, 23(2), 670-674.

Lee, H. J., Jung, B., Kang, Y. S. & Lee, H. (2004). Phase separation of polymer casting solution by nonsolvent vapor, J. Membrane Sci., 245(1-2), 103-112.

Love, C. T. (2011). Thermomechanical analysis and durability of commercial microporous polymer Li-ion battery separators. J. Power Sources 196(5), 2905-2912.

Matsuba, G., Kaji, K., Nishida, K., Kanaya, T. & Imai, M. (1999). Conformational change and orientation fluctuations of isotactic polystyrene prior to crystallization, Polym. J. 31(9), 722-727.

Mazich, K. A. & Carr, S. H. (1983). Effect of flow on the miscibility of a polymer blend. J. Appl. Phys. 54(10), 5511-5514.

Mikos, A. G. & Temenoff, J. S. (2000). Formation of highly porous biodegradable scaffolds for tissue engineering. Electron. J. Biotechnol. 3(2), 1-6.

Olmsted, P. D.; Poon, W. C. K.; McLeish, T. C. B.; Terrill, N. J. & Ryan, A. J. (1998). Spinodal-assisted crystallization in polymer melts, Phys. Rev. Lett. 81, 373-376.

Phulkerd, P., Hagihara, H., Nobukawa, S., Uchiyama, Y. & Yamaguchi, M. (2013). Plastic deformation behavior of polypropylene sheet with transversal orientation. J. Polym. Sci. Polym. Phys. Ed. 51 (11), 897-906.

Rangel-Nafaile, C., Metzner, A. B. & Wissbrun, K. F. (1984). Analysis of stress-induced phase separations in polymer solution. Macromolecules 17(6), 1187-1195.

Richter, I., Sun, P. C., Xu, F., & Fainman, Y. (1995). Design considerations of form birefringent microstructures. Appl. Opt.34(14), 2421-2429.

Samthong, C., Seemork, S., Nobukawa, S., Yamaguchi, M., Praserthdam, P. & Somwangthanaroj, A.

(2014). Morphology, structure and properties of poly(lactic acid) microporous films containing poly(butylene terephthalate) fine fibers fabricated by biaxial stretching. J. Appl. Polym. Sci., in press (early view), DOI 10.1002/app.41415.

Selvam, S., Chang, W. V., Nakamura, T., Samant, D. M., Thomas, P. B., Trousdale, M. D. et al. (2009). Microporous poly(L-Lactic acid) membranes fabricated by polyethylene glycol solvent-cast/particulate leaching technique, Tissue Eng. Part C, 15(3), 463-474.

Silverstein, M. S., Cameron, N. R. & Hillmyer, M. A. Porous Polymers, 2011, Wiley, Hoboken.

Songsurang, K., Miyagawa, A., Abd Manaf, M. E., Phulkerd, P., Nobukawa, S. & Yamaguchi, M. (2012). Optical anisotropy in solution-cast film of cellulose triacetate, Cellulose, 20(1), 83-96.

Treloar, L. R. G. The Physics of Rubber Elasticity, 1958, Clarendon Press, Oxford.

Wakao, N. & Smith, J. M. (1964). Diffusion and reaction in porous catalysts. Ind. Eng. Chem. Fundam, 3(2), 123-127.

Yamaguchi, M., Okada, K., Abd Manaf, M. E., Shiroyama, Y., Iwasaki, T. & Okamoto, K. (2009). Extraordinary wavelength dispersion of orientation birefringence for cellulose esters. Macromolecules, 42(22), 9034–9040.

Yamaguchi, M., Abd Manaf, M. E., Songsurang, K. & Nobukawa, S. (2012). Material design of retardation films with extraordinary wavelength dispersion of orientation birefringence, Cellulose 19(3), 601–613.

Yanase, H., Moldenaers, P., Mewis, J., Abetz, V., Van Egmond, J. & Fuller, G. G. (1991). Structure and dynamics of a polymer solution subject to flow-induced phase separation. Rheol. Acta, 30(1), 89-97.

Figure Captions

Figure 1 Chemical structure of (a) CTA, (b) DEP, and (c) DIDA.

Figure 2 Temperature dependence of dynamic tensile moduli such as storage modulus *E'* and loss modulus *E"* at 10 Hz for pure CTA and plasticized CTA films with 10 phr of DEP and DIDA.

Figure 3 Stress-strain curves of the films stretched at T_{draw}. The strain rate is 0.05 s^{-1}.

Figure 4 Wavelength dependence of birefringence for the pure CTA and plasticized CTA films with a draw ratio of 1.5.

Figure 5 SEM pictures of cut surface of the films after extraction; (a) CTA/DEP and (b) CTA/DIDA.

Figure 6 Wavelength dependence of birefringence for the stretched films before/after extraction; (a) CTA, (b) CTA/DEP and (c) CTA/DIDA. The films were stretched at a draw ratio of 1.5 at a strain rate of 0.5 s^{-1}.

Figure 7 Birefringence of the stretched film with ellipsoidal pores.

Figure 8 Growth of porous structure in the CTA/DIDA film; Phase separation occurs at heating and stretching processes.

Figure 9 Stress-strain curves at various strain rates; (a) CTA and (b) CTA/DIDA.

Figure 10 Wavelength dependence of birefringence (a) CTA films after extraction and (b) CTA/DIDA films before/after extraction. The films were stretched at a draw ratio of 1.5 at various strain rates.

Table 1 Characteristics of samples.

	CTA	Plasticizer	
		DEP	DIDA
Solubility parameter ($(MPa)^{1/2}$)	19.4	20.7	17.0
Refractive index (-)	1.48	1.50	1.45

Table 2 Glass transition temperature and drawing temperature for the films.

	CTA	CTA/DEP	CTA/DIDA
T_g (°C)	195	151	192
T_{draw} (°C)	213	178	208

Table 3 Total transmittance of annealed CTA/DIDA films with various annealing time.

	Annealing time /min			
	0	1	10	20
CTA	92.38	91.60	91.19	91.81
CTA/DIDA	92.55	90.88	90.06	89.41

(a)

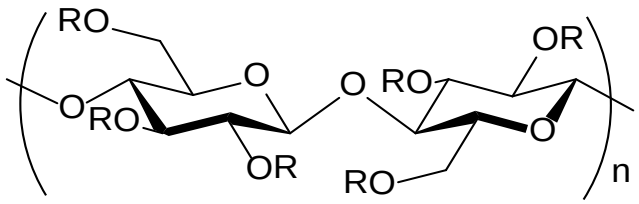

R= $COCH_3$

(b)

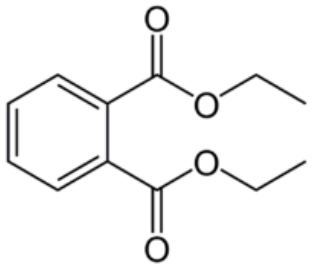

(c)

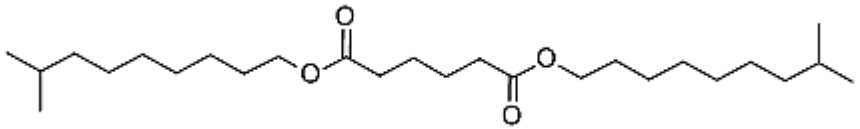

Figure 1

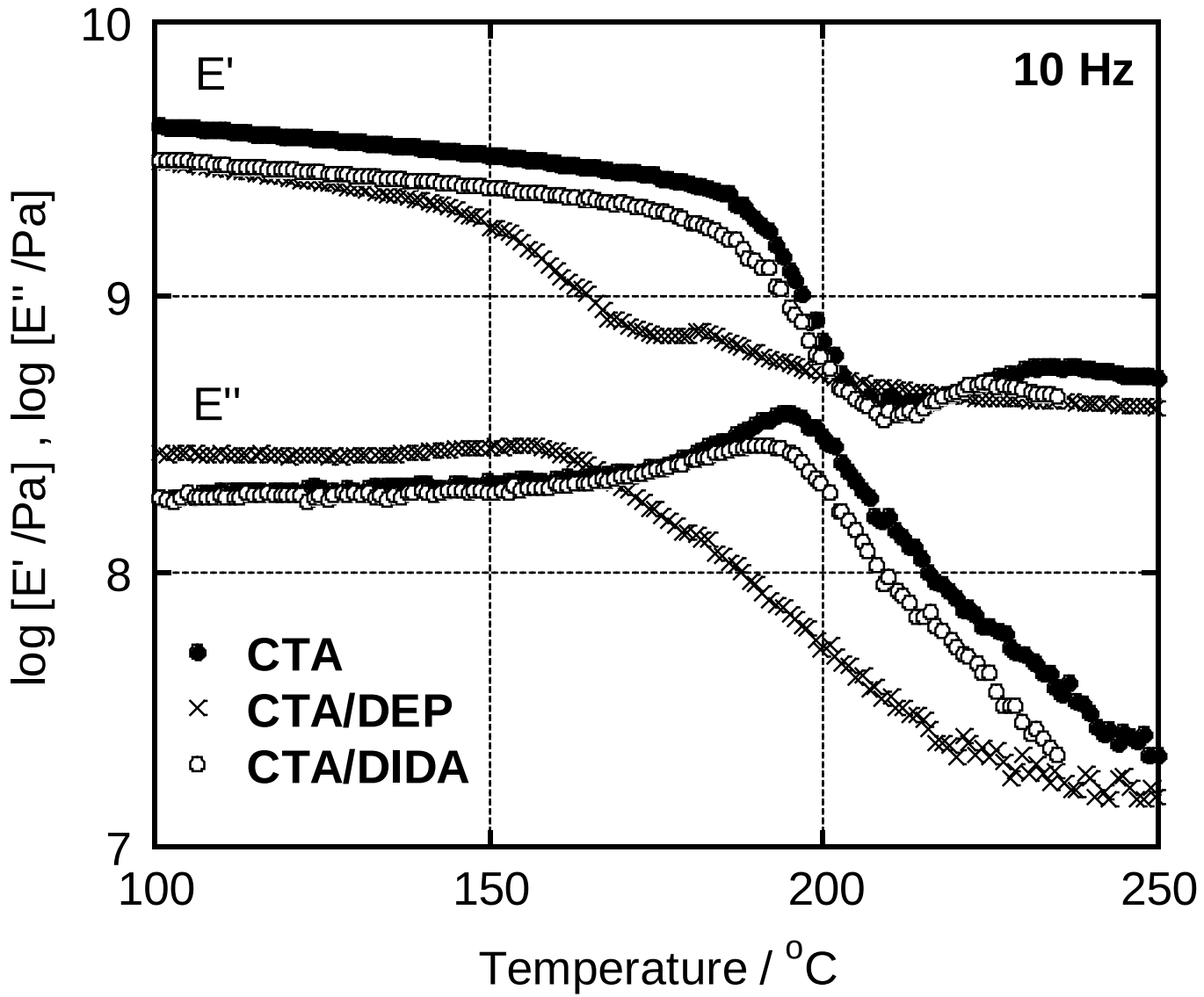
10
9
8
7
E'
10 Hz
E''
CTA
CTA/DEP
CTA/DIDA
log [E' /Pa] , log [E'' /Pa]
100
150
200
250
Temperature / °C

Figure 2

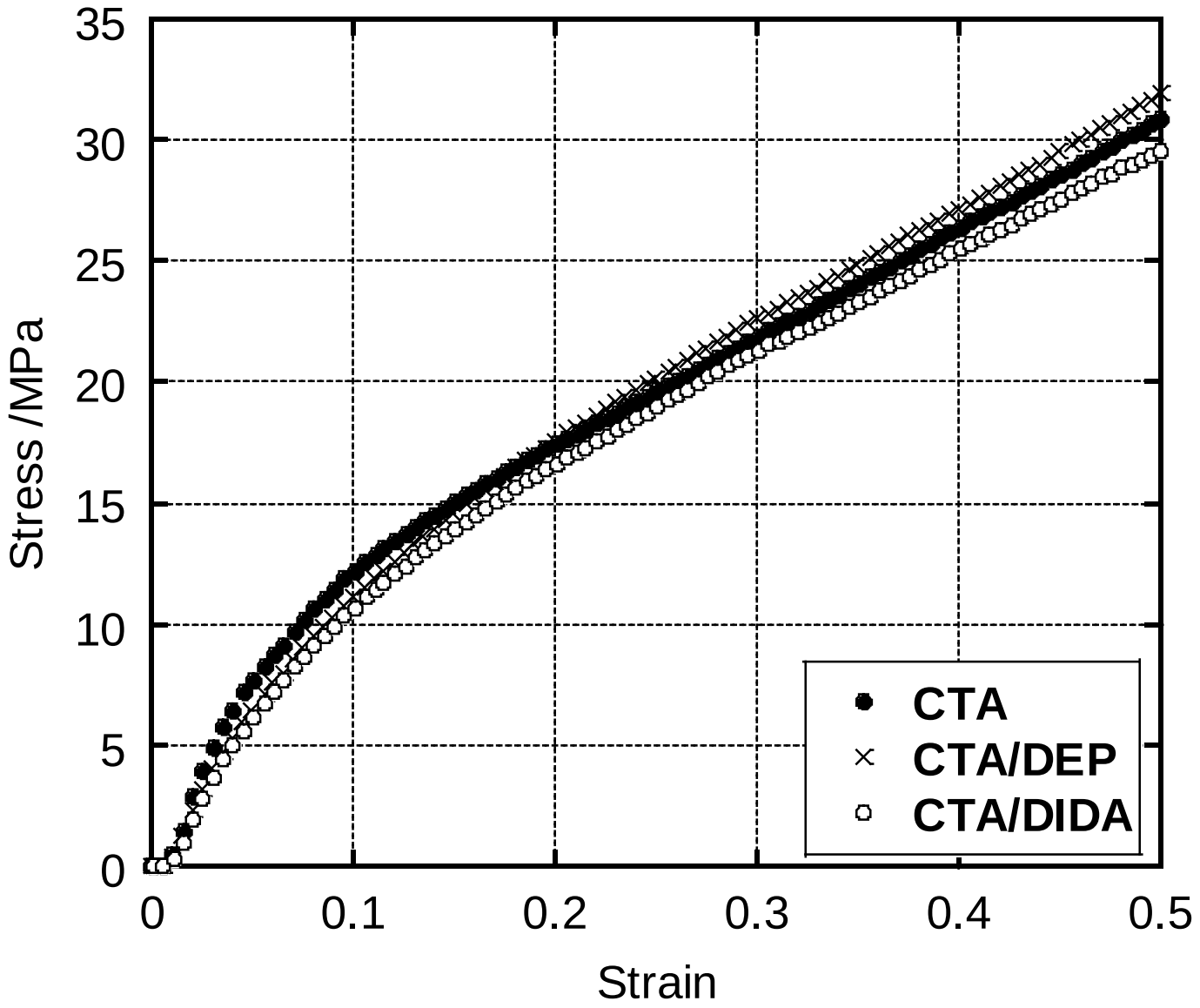
35
30
25
20
15
10
5
0
Stress /MPa
0
0.1
0.2
0.3
0.4
0.5
Strain
CTA
CTA/DEP
CTA/DIDA

Figure 3

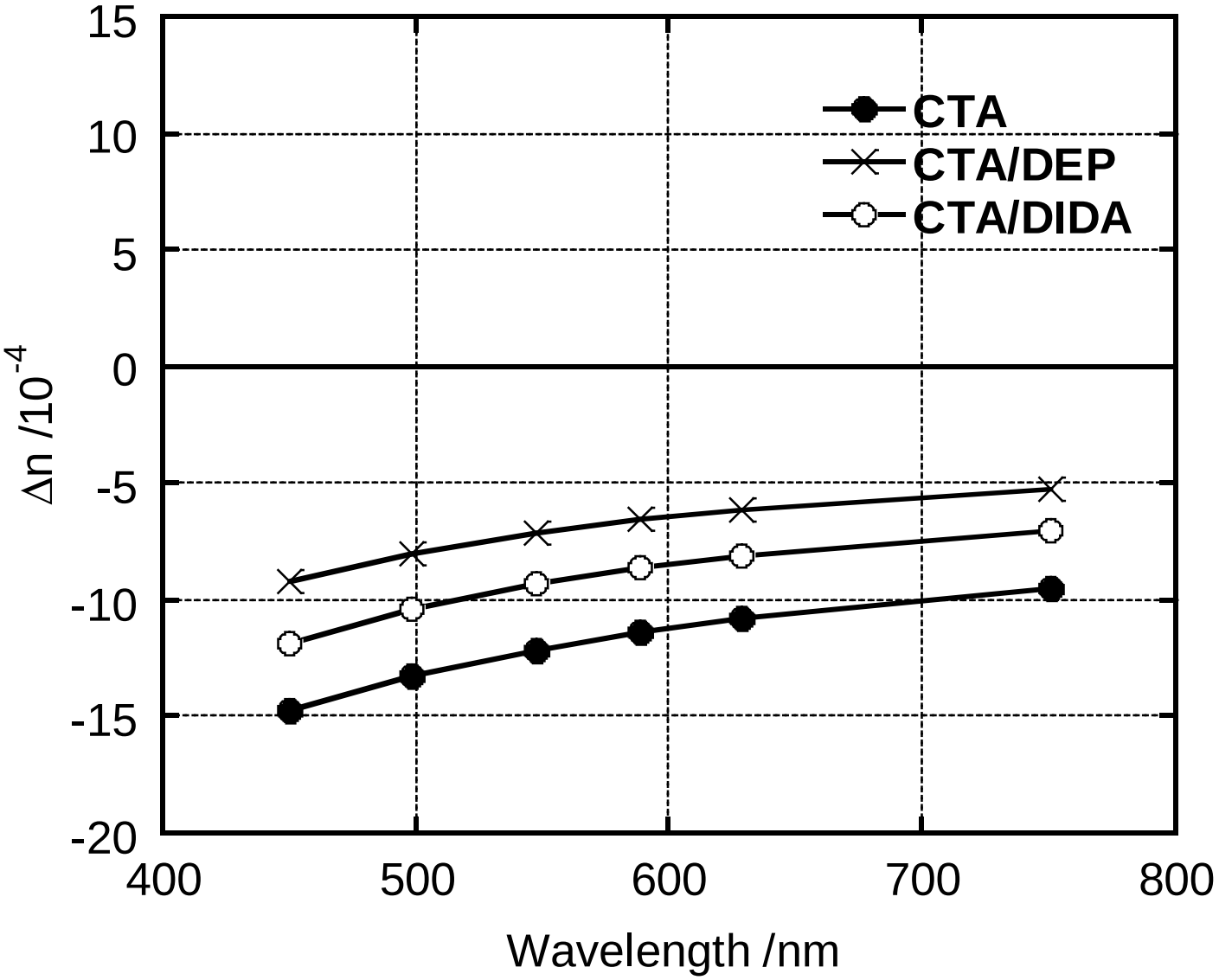
15
10
5
0
-5
-10
-15
-20
Δn /10-4
400
500
600
700
800
Wavelength /nm
CTA
CTA/DEP
CTA/DIDA

Figure 4

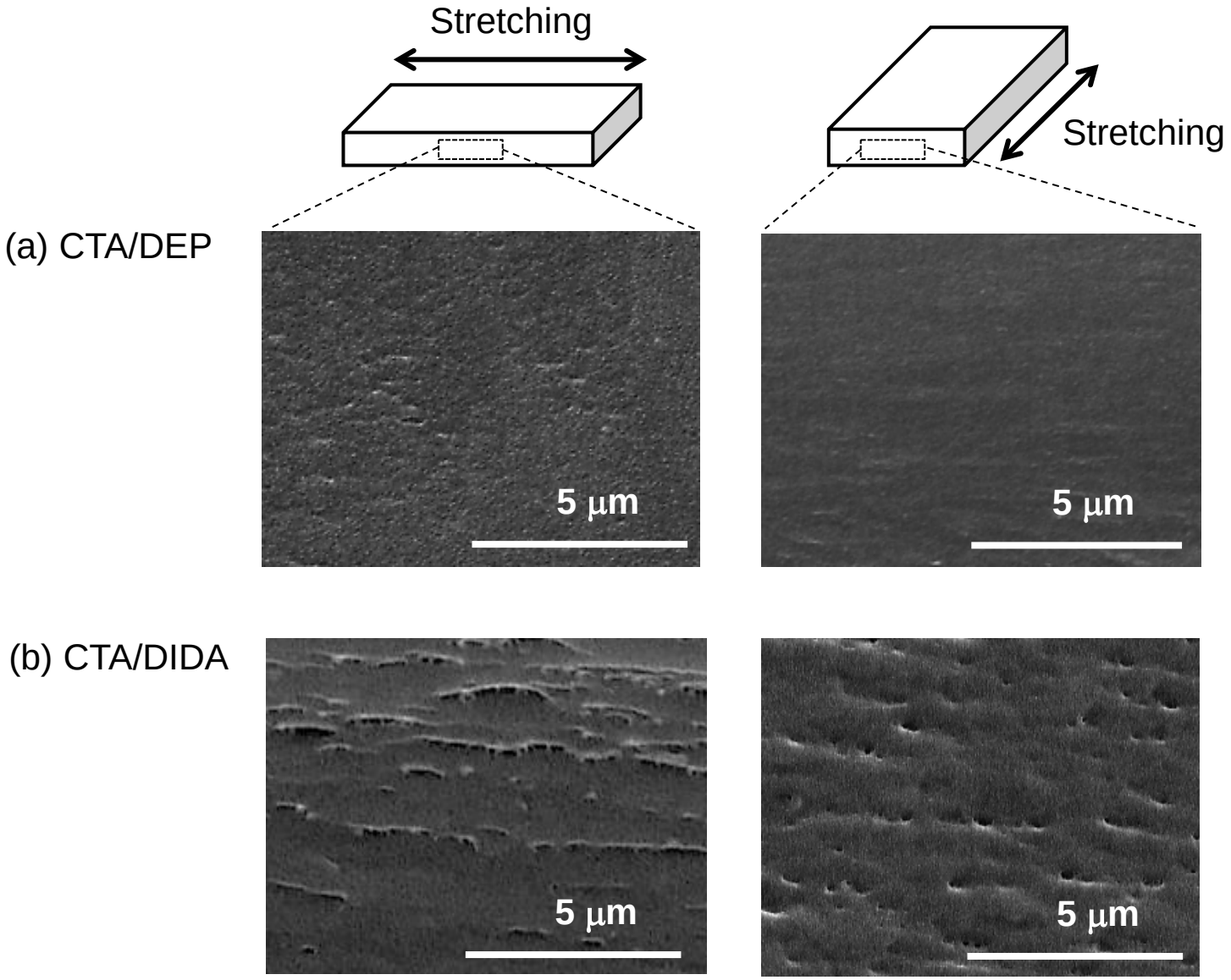

Figure 5

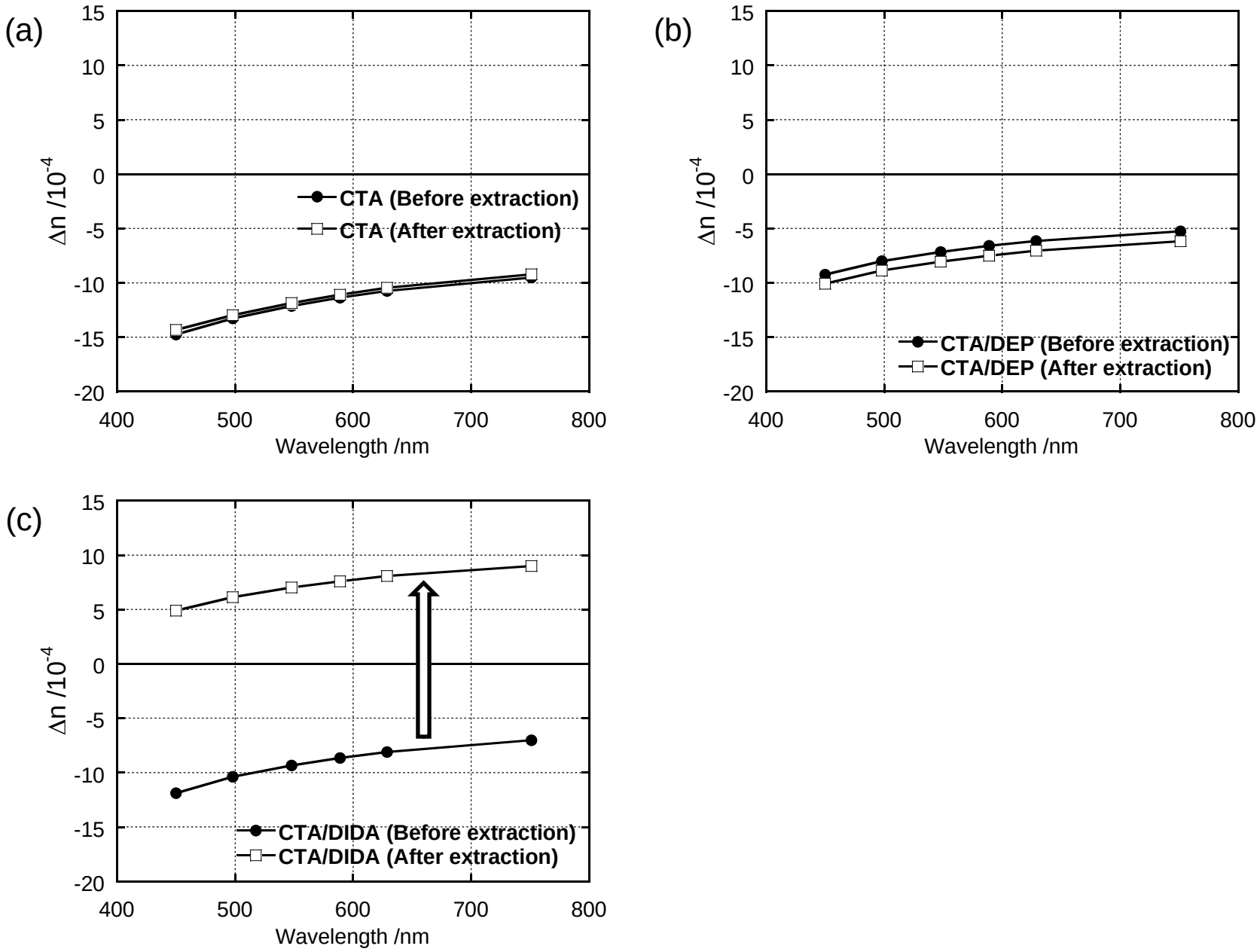
(a)
15
10
5
0
-5
-10
-15
-20
Δn /10-4
400
500
600
700
800
Wavelength /nm
CTA (Before extraction)
CTA (After extraction)
(b)
CTA/DEP (Before extraction)
CTA/DEP (After extraction)
(c)
CTA/DIDA (Before extraction)
CTA/DIDA (After extraction)

Figure 6

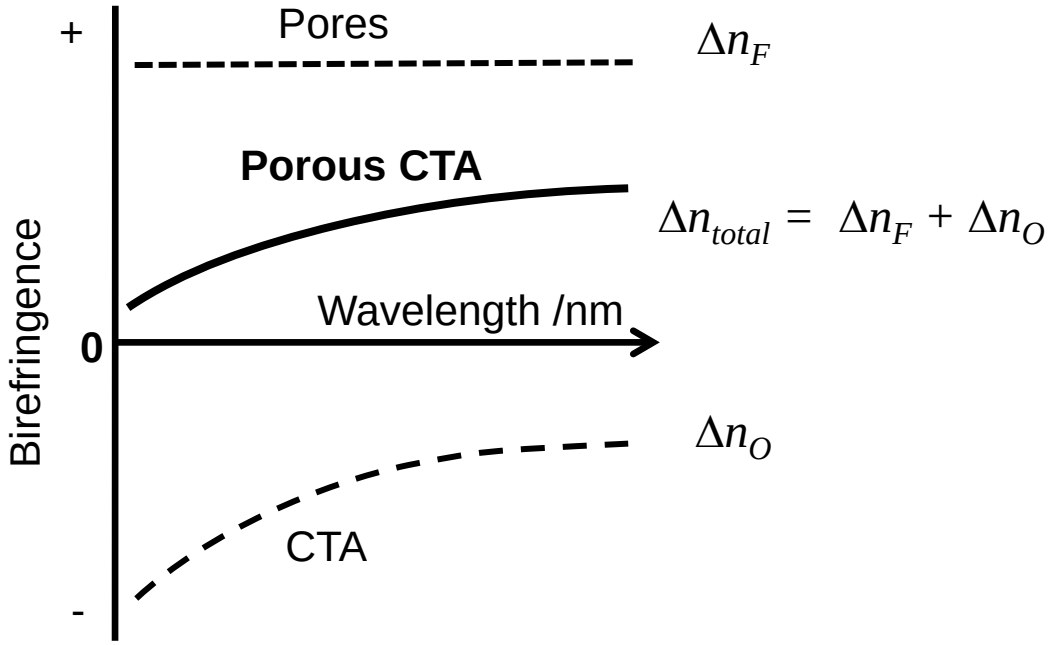
+
Pores
Δn_F
Porous CTA
$\Delta n_{total} = \Delta n_F + \Delta n_O$
Birefringence
Wavelength /nm
0
Δn_O
CTA
-

Figure 7

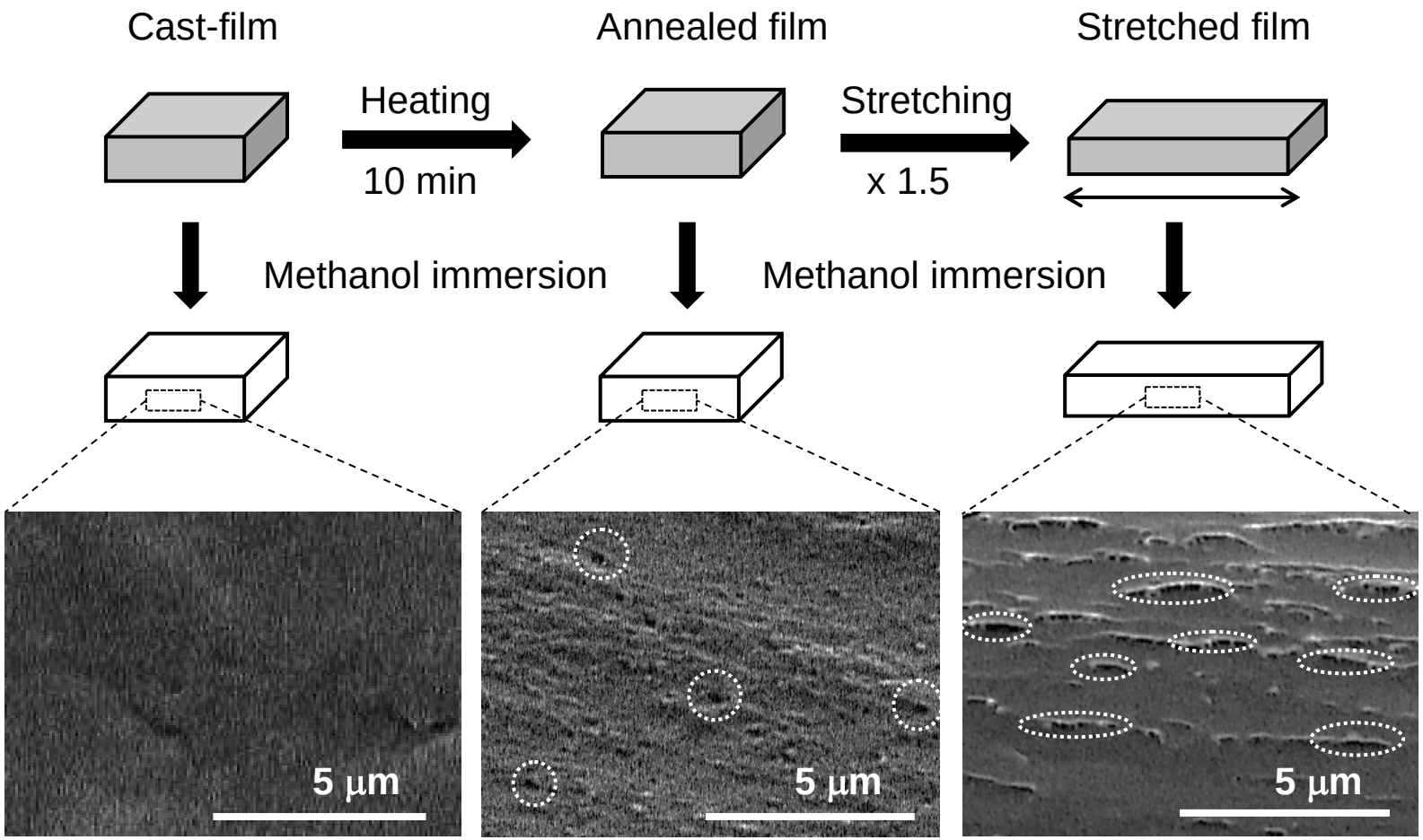
Cast-film
Annealed film
Stretched film
Heating
10 min
Stretching
x 1.5
Methanol immersion
Methanol immersion
5 μm
5 μm
5 μm

Figure 8

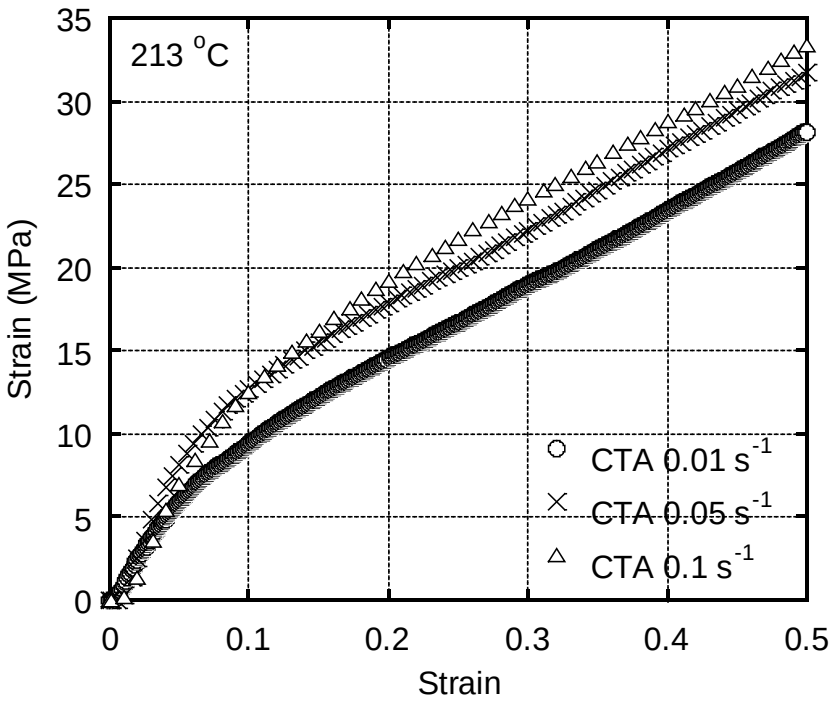
213 °C
Strain (MPa)
Strain
CTA 0.01 s-1
CTA 0.05 s-1
CTA 0.1 s-1
0
5
10
15
20
25
30
35
0
0.1
0.2
0.3
0.4
0.5

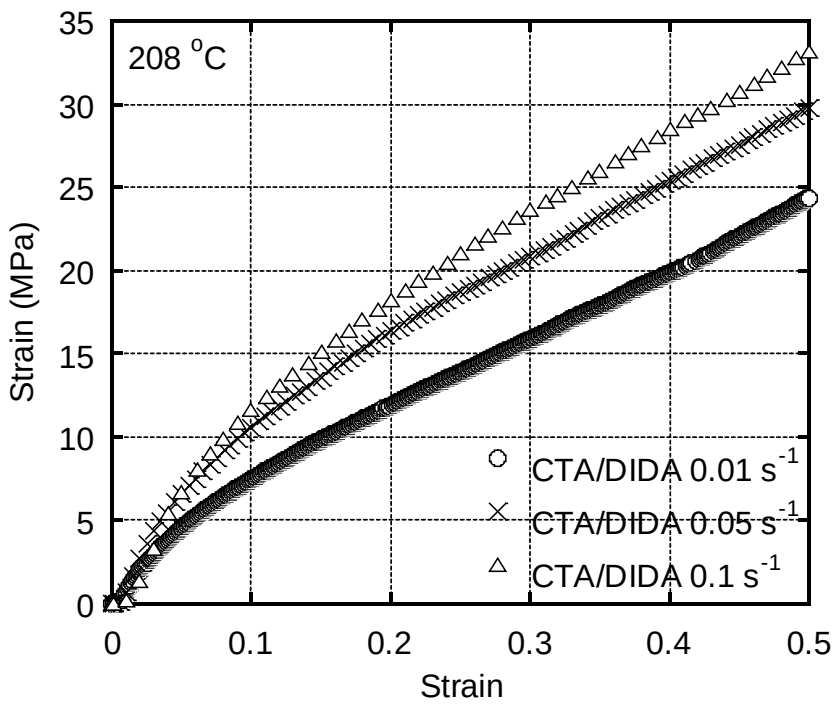
208 °C
Strain (MPa)
Strain
CTA/DIDA 0.01 s-1
CTA/DIDA 0.05 s-1
CTA/DIDA 0.1 s-1
0
5
10
15
20
25
30
35
0
0.1
0.2
0.3
0.4
0.5

Figure 9

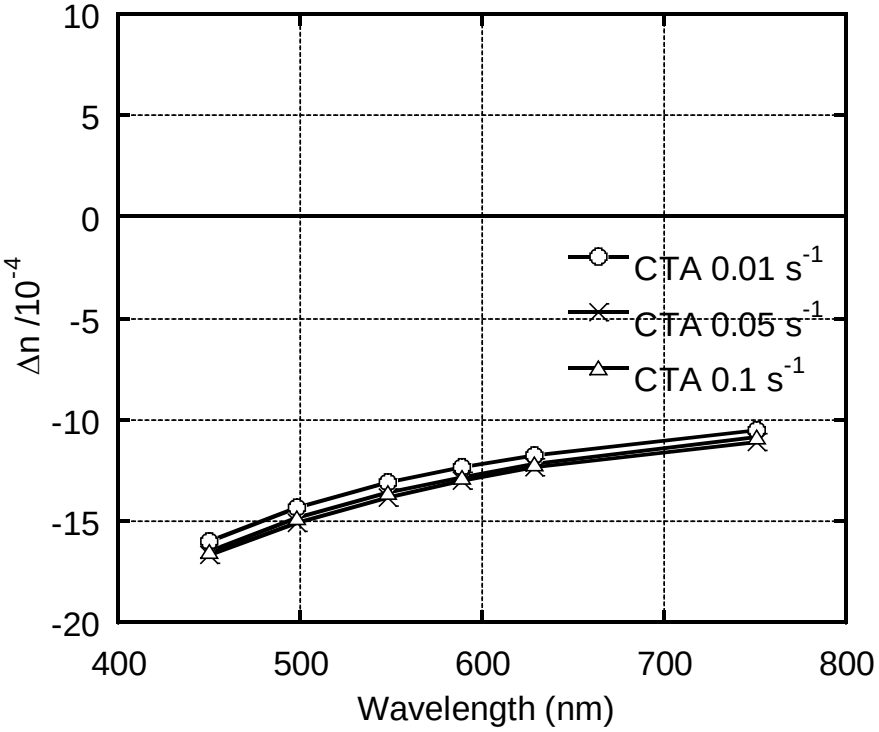
10
5
0
-5
-10
-15
-20
400
500
600
700
800
Wavelength (nm)
Δn /10-4
CTA 0.01 s-1
CTA 0.05 s-1
CTA 0.1 s-1

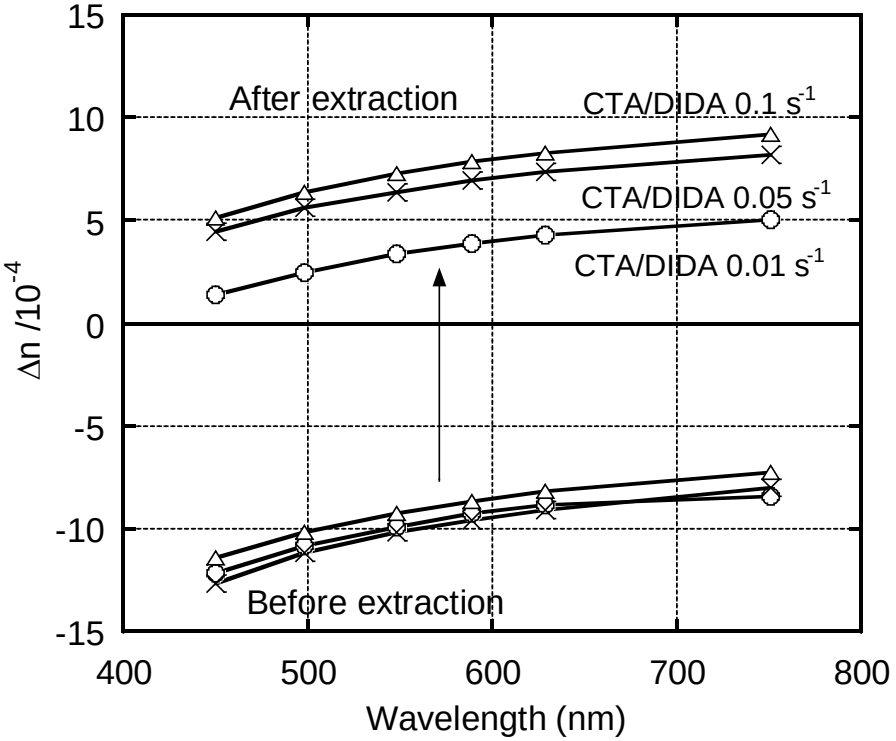
15
10
5
0
-5
-10
-15
400
500
600
700
800
Wavelength (nm)
Δn /10-4
After extraction
CTA/DIDA 0.1 s-1
CTA/DIDA 0.05 s-1
CTA/DIDA 0.01 s-1
Before extraction

Figure 10